Research Article Vol. 13, No. 8 / 1 Aug 2023 / Optical Materials Express 2449

Optical Materials EXPRESS

Improving the hole injection efficiency in AlGaN DUV LEDs by minimizing the band offset at the p-EBL/hole supplier interface

WENTAO TIAN,[1,2] MENGRAN LIU,[1,2] SHUTI LI,[3] AND CHAO LIU[1,2,*]

[1] School of Microelectronics, Institute of Novel Semiconductors, Shandong Technology Center of Nanodevices and Integration, State Key Laboratory of Crystal Materials, Shandong University, Jinan 250100, China

[2] Shenzhen Research Institute, Shandong University, Shenzhen 518057, China

[3] Guangdong Engineering Research Center of Optoelectronic Functional Materials and Devices, Institute of Semiconductors, South China Normal University, Guangzhou, 510631, China

[*] chao.liu@sdu.edu.cn

Abstract: In AlGaN-based deep ultraviolet light-emitting diodes (DUV LEDs), the large valence band offset between the Al-rich electron blocking layer (EBL) and p-AlGaN hole supplier weakens the chance of holes being injected into the active region. Only holes with kinetic energy larger than the barrier height at the EBL/p-AlGaN interface are allowed to climb over the EBL before entering the active region, limiting the hole injection efficiency and thus reducing the external quantum efficiency (EQE). In this work, we incorporate a thin AlGaN insertion layer between EBL and the p-AlGaN hole supplier to enhance the hole injection efficiency of DUV LEDs via regulating the energy band at the p-EBL/p-AlGaN interface. By systematically investigating and analyzing the effects of aluminum components in the insertion layers on the hole injection and the electron confinement, we found that the insertion layer with an Al composition of 45% can effectively enhance the EQE of DUV LEDs by 40.5% and suppress efficiency droop by 65.5%. The design strategy provides an effective approach to boost the hole injection efficiency for AlGaN-based DUV LEDs.

1. Introduction

Featured with long lifetime, compact volume, and environmental friendliness, AlGaN-based ultraviolet light-emitting diodes (DUV LEDs) have been perceived as the most promising candidate for the next-generation light sources [1–4]. However, the optical power and external quantum efficiency (EQE) of DUV LEDs are still far from satisfactory [5–8], which severely hinders the commercial application of AlGaN-based DUV LEDs. Extensive research has revealed that the inferior performance of DUV LEDs primarily originates from serious electron leakage and insufficient hole injection [9–13]. The common strategy for diminishing electron leakage is the employment of the p-type high-Al-content electron blocking layer (p-EBL) between the last quantum barrier (LQB) and p-type hole supplier [14]. Nevertheless, the large lattice mismatch between LQB and Al-rich p-EBL induces the polarization related positive sheet charges at the LQB/p-EBL interface that can reflect the holes from the p-type hole supplier, thus reducing the hole injection efficiency of DUV LEDs [15,16]. Moreover, the Al-rich p-EBL also introduces an additional potential barrier for holes in the valence band that severely hampers the holes from overflowing into the active region [17], which is also deleterious for the hole injection. To promote hole injection into the active region, extensive research has put forward a variety of p-EBL structures with reduced potential barrier height for holes, including w-shaped p-EBL [18], heterojunction p-EBL [19], and anti-trapezoidal p-EBL [20]. Specifically, Chu *et al.* reported that

#494404 https://doi.org/10.1364/OME.494404
Journal © 2023 Received 1 May 2023; revised 25 Jun 2023; accepted 27 Jun 2023; published 1 Aug 2023

Optical Materials EXPRESS

the p-EBL with a low-Al-composition AlGaN insertion layer presents the advantage of increasing the tunneling probability for holes and enhancing the hole transport capability into the active region [21]. In addition, the hole injection efficiency can also be improved when the AlGaN/GaN superlattice p-EBL and Al-graded p-EBL are adopted, as the polarization-enhanced ionization of Magnesium (Mg) acceptor facilitates the hole injection from the hole supplier [22–24]. On the other hand, modifying the energy band diagram at the vicinity of the LQB/p-EBL interface is another feasible approach to reduce the hole blocking effect by the Al-rich p-EBL. It has been demonstrated that utilizing a step-graded AlInGaN LQB lattice-matched to the p-EBL layer favors the lessening of hole depletion around the LQB/p-EBL interface [25], attributing to the eliminated positive polarization charges between the LQB and p-EBL layers. Liu et al. proposed an Al-composition-increasing AlGaN layer (ACI-AlGaN) inserted between the LQB and p-EBL to introduce negative sheet charges at LQB/p-EBL interface [26], which can further enhance the hole injection efficiency. Other than the LQB/p-EBL interface, the interface between p-EBL and p-AlGaN hole supplier should also be taken into account. Despite of the intrinsic negative sheet charges at the p-EBL/p-AlGaN interface that is naturally favorable for the hole injection, the large valence band offset between Al-rich p-EBL and p-AlGaN hole supplier tends to block the holes from the hole supplier, resulting in insufficient hole injection. However, the hole transport behavior across the p-EBL/p-AlGaN interface is still unclear so far, and the corresponding design strategy of the heterointerface remains to be explored for the purpose of achieving satisfactory hole injection efficiency.

In this paper, we analyze the effect of the barrier height at the p-EBL/p-AlGaN interface on the carrier transport behavior and investigate the underlying mechanism behind the improved optical and electrical characteristics of the DUV LEDs. In addition, we propose a potential approach to improve the hole injection efficiency of DUV LEDs by embedding a thin $Al_xGa_{1-x}N$ layer between p-EBL and p-AlGaN hole supplier. The incorporation of a thin $Al_xGa_{1-x}N$ layer ameliorates the valence band offset between p-EBL and p-AlGaN hole supplier and promotes hole accumulation at p-EBL/p-AlGaN interface, facilitating the holes transport into the active region. By optimizing the Al composition of the inserted thin $Al_xGa_{1-x}N$ layer, we found that the proposed DUV LED with an $Al_{0.45}Ga_{0.55}N$ thin insertion layer exhibits enhanced EQE by 40.47% at the injection current density of 150 A/cm^2 compared with the reference structure. The results provide an effective way to obtain high-efficiency AlGaN-based DUV LEDs.

2. Device structure and parameters

The Schematic diagram of the AlGaN-based DUV LED structures used in this work is presented in Fig. 1(a). The reference architecture comprises an n-$Al_{0.6}Ga_{0.4}N$ layer with electron concentration of 8×10^{18} cm^{-3}, followed by 5 pairs of multiple quantum wells (MQWs), which consist of 3-nm-thick $Al_{0.45}Ga_{0.55}N$ quantum wells and 10-nm-thick $Al_{0.57}Ga_{0.43}N$ quantum barriers. The MQW active region is capped with a 10-nm-thick p-$Al_{0.6}Ga_{0.4}N$ EBL, followed by a 50-nm-thick p-$Al_{0.4}Ga_{0.6}N$ layer and a 50-nm-thick p-GaN layer as the hole supplier. The effective hole concentration for the p-type hole supplier is set to be $\sim 1 \times 10^{17}$ cm^{-3}. As for the proposed DUV LEDs, they feature the same epitaxial structures except that a thin $Al_xGa_{1-x}N$ insertion layer is introduced between the p-EBL and p-$Al_{0.4}Ga_{0.6}N$ hole supplier. The Al composition (x) in the thin insertion layer is varied among the proposed structures, which is set to be 0.35, 0.45, 0.55, and 0.65 for Device A, B, C, and D, respectively. The area of the mesa is set to be 350 µm × 350 µm for all the devices. In addition, the carrier transport behavior in the p-type region for the reference structure and proposed structure is elaborated in Fig. 1(b). It can be observed that there exists a large valence band offset/barrier height (ΔE_1) at the p-EBL/p-$Al_{0.4}Ga_{0.6}N$ interface. Only the holes with kinetic energy (E_k) larger than ΔE_1 are able to be injected into the p-EBL from the p-$Al_{0.4}Ga_{0.6}N$ and p-GaN hole supplier. In the reference structure, the probability (P_h) of holes

Optical Materials EXPRESS

being injected into the p-EBL can be calculated using the following equation [27]:

$$P_h = \int_{E\geq \max\{0,\ \Delta E_1 - E_k\}}^{+\infty} F(E)\cdot P(E)dE \Big/ \int_0^{+\infty} F(E)\cdot P(E)dE, \tag{1}$$

in which F(E) represents the probability of holes occupying a quantum state at energy E, P(E) is the valence band density of states in the p-AlGaN layer. As for the proposed structures with an insertion layer, it can be found that the incorporation of a thin $Al_xGa_{1-x}N$ layer modifies the energy band diagram at the p-EBL/p-AlGaN interface and divides ΔE_1 into two sections, including the barrier height (ΔE_{1a}) at $Al_xGa_{1-x}N$/p-AlGaN interface and the barrier height (ΔE_{1b}) at p-EBL/$Al_xGa_{1-x}N$ interface. Accordingly, the probability of holes being injected into the EBL is

$$P_h = \int_{E\geq \max\{0,\ \Delta E_{1i} - E_k\}}^{+\infty} F(E)\cdot P(E)dE \Big/ \int_0^{+\infty} F(E)\cdot P(E)dE, \tag{2}$$

in which the ΔE_{1i} represents the max $\{\Delta E_{1a}, \Delta E_{1b}\}$. Moreover, when the holes arrive at the p-EBL from p-AlGaN hole supplier, the effective valence band barrier height of p-EBL ($\Delta\Phi_H$) becomes another obstacle for hole injection into the MQW active region. The effective valence band barrier height can be calculated by

$$\Delta\Phi_H = \Delta E_2 - kT * ln(p_{EBL}/N_v), \tag{3}$$

$$\Delta E_2 = E_{v\_EBL} - E_{v\_LQB}, \tag{4}$$

in which p_{EBL} and N_v represent the hole concentration in p-EBL and the effective density of states for holes in the p-EBL layer, respectively. ΔE_2 is the valence band offset between LQB and p-EBL. E_{v_LQB} denotes the valence band edge of LQB.

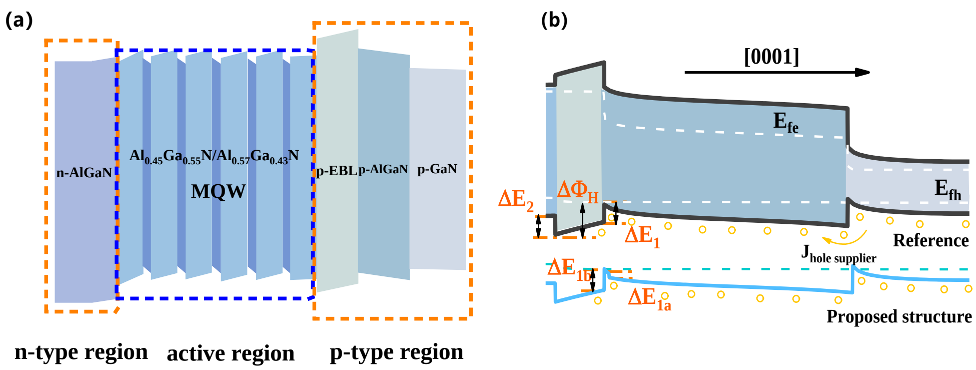

Fig. 1. (a) Schematic diagram for the reference structure, including the n-type region, the active region, and the p-type region. (b) Schematic energy band diagram of p-type region in the reference structure and proposed structure. Yellow circles illustrate the holes at the p-type region. ΔE_1 and ΔE_2 represent the valence band offset/barrier height at p-EBL/p-$Al_{0.4}Ga_{0.6}N$ interface and LQB/p-EBL interface, respectively. Φ_H means the effective valence band height of p-EBL. E_{fe} is the quasi-Fermi level for electrons and E_{fh} is the quasi-Fermi level for holes. ΔE_{1b} and ΔE_{1a} are the barrier height at p-EBL/$Al_xGa_{1-x}N$ interface and $Al_xGa_{1-x}N$/p-AlGaN interface, respectively.

It can be induced through Eq. (1) that the reduced barrier height (ΔE_1) between p-EBL and p-AlGaN hole supplier is beneficial for improving the probability of holes to be injected into the p-EBL and enhancing the hole concentration in the p-EBL layer, which is in favor of reducing the Φ_H (as depicted from Eq. (3)) and thus improving hole injection efficiency into the MQW region. Therefore, reducing the barrier height (ΔE_1) between p-EBL and p-AlGaN hole supplier

Optical Materials EXPRESS

is effective for transporting holes from the hole supplier into the active region and improving the optical characteristics of AlGaN-based DUV LEDs.

We utilize the Advanced Physical Models of Semiconductor Devices (APSYS) simulation software to elaborate the effect of the $Al_xGa_{1-x}N$ insertion layer on the carrier transport behavior as well as the device characteristics by solving the Schrödinger equation, Poisson's equation, and current continuity equations. In this work, the band offset between the conduction band and valence band for AlGaN/AlGaN heterostructure was set as 50:50 [28]. The light extraction efficiency, Shockley-Read-Hall recombination lifetime, and Auger recombination coefficient were set to be 6%, 14 ns, and 1.7×10^{-30} cm^6/s, respectively. Besides, the detailed material parameters used during the simulation can be found in Ref. [29]. The non-local quantum well (QW) transport model [30] and interband tunneling model [31] are also taken into consideration in the calculation process.

3. Results and discussions

The EQE and optical power of the investigated devices are presented in Fig. 2(a) and 2(b), respectively. Please note that the numerically calculated EQE and optical power of the reference structure are consistent with the experimentally measured results (denoted as dot) from Ref. [32], manifesting the effectiveness of the physical models employed in the simulation. As shown in Fig. 2, Device A with an $Al_{0.35}Ga_{0.45}N$ insertion layer not only exhibits deteriorative optical power, but also shows severe efficiency droop (efficiency droop = $\frac{EQE_{max}-EQE_J}{EQE_{max}}$, in which EQE_{max} and EQE_J represent the peak value of EQE and the EQE at the injection current density of J, respectively) in comparison to the reference structure. On the contrary, Device B with $Al_{0.45}Ga_{0.55}N$ insertion layer and Device C with $Al_{0.55}Ga_{0.45}N$ insertion layer possess remarkably enhanced optical power and EQE. Specifically, the light output power of Device B is improved by 40.5% at the injection current density of 150 A/cm^2 and the corresponding efficiency droop is reduced by 60.5%, as compared with those from the reference structure. However, with further increased Al% to 65% in the insertion layer, the EQE of Device D features obvious droop behavior at high injection current density. Therefore, the optical performance of DUV LEDs can be improved by inserting a thin layer with appropriate Al component between the EBL and the p-AlGaN hole supplier.

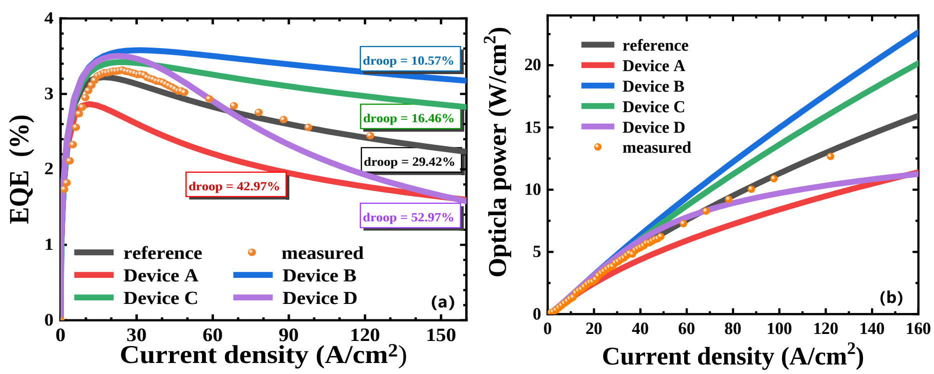

Fig. 2. (a) Calculated EQE and (b) optical power for measured structure and proposed structure Device A, B, C, and D, respectively.

For the purpose of clarifying the in-depth mechanism with regard to the improvement of device performance, the valence band diagrams of the investigated structures are displayed in Fig. 3(a)–3(e), in which the hole transport behavior from the p-type hole supplier to the LQB layer

Optical Materials EXPRESS

is also illustrated. To further explore the effect of the proposed structure on the hole injection, the hole concentration of the p-EBL for the investigated structures is displayed in Fig. 3(f). In addition, we extract the barrier height at $Al_xGa_{1-x}N$/p-AlGaN interface (ΔE_{1a}), band barrier height at p-EBL/$Al_xGa_{1-x}N$ interface (ΔE_{1b}), the effective valence band barrier height of p-EBL (Φ_H), the effective conduction band height of p-EBL (Φ_C) and the effective barrier height for electrons of the AlGaN insertion layer (Φ_{C1}) among the investigated devices. The detailed values of these parameters are displayed in Table 1.

Table 1. The Value Of ΔE_{1b}, ΔE_{1a}, Φ_C, Φ_H, Φ_{C1} and σ

	ΔE_{1b} (meV)	ΔE_{1a} (meV)	Φ_H (meV)	Φ_C (meV)	Φ_{C1} (meV)	σ (m^{-2})
Ref.	-	-	471.2	376.5	-	-
Device A	273	−108.4	484.6	363.6	−41.6	-6.4×10^{16}
Device B	170.3	97.2	445.9	408.1	160.6	-4×10^{16}
Device C	58.4	160	461.6	383.9	298.3	-1.4×10^{16}
Device D	−59.6	314.7	499.4	287.3	421.9	1.5×10^{16}

As for the reference structure shown in Fig. 3(a), before being injected into the active region, holes from the p-$Al_{0.4}Ga_{0.6}N$ hole supplier need to climb over the potential barrier (ΔE_1) of 222.6 meV at the p-EBL/p-AlGaN interface. Besides, the large effective valence band barrier height of 471.2 meV also reduces thermionic emission (T_E) efficiency of holes across the p-EBL. As for the proposed structures with AlGaN insertion layer, it can be seen from Table 1 that the barrier height (ΔE_{1b}) at the p-EBL/$Al_{0.35}Ga_{0.55}N$ interface (I_2) of Device A is 273 meV, which is larger than ΔE_1 of the reference structure. These results are attributed to the energy band discontinuity between p-EBL and $Al_{0.35}Ga_{0.65}N$ layer in Device A which is more severe than that between p-EBL and p-$Al_{0.4}Ga_{0.6}N$ hole supplier in the reference structure, as show in Fig. 3(b). It is indicated through Eq. (2) that the large barrier height (ΔE_{1b}) reduces the probability of the holes climbing over the p-EBL, which results in the diminution of the hole current from the hole supplier to the active region. Accordingly, as presented in the inset of Fig. 3(b), numerous holes are confined in the inserted $Al_{0.35}Ga_{0.65}N$ layer by the high barrier height (ΔE_{1b}) at interface I_2, leading to reduced hole concentration in p-EBL of Device A (Fig. 3(f)). Moreover, the effective valence band barrier height of p-EBL is also increased from 471.2 meV for the reference structure to 484.6 meV for Device A, which is detrimental for transporting holes into the active region.

With increased Al composition in the insertion layer of Device B in Fig. 3(c), the energy band discontinuity between p-EBL and $Al_{0.45}Ga_{0.55}N$ layer is reduced so that a lower barrier height (ΔE_{1b}) is recorded at interface I_4 of Device B than ΔE_1 of the reference structure, as depicted in Table 1. Thus, the probability of holes being injected into the p-EBL can be potentially raised. From the inset of Fig. 3(c), it can be found that the hole concentration at both the p-EBL/$Al_{0.45}Ga_{0.55}N$ interface (I_4) and $Al_{0.45}Ga_{0.55}N$/p-AlGaN interface (I_3) of Device B is smaller than that at the p-EBL/p-AlGaN interface (I_0) of the reference structure. Correspondingly, Fig. 3(f) shows that Device B possesses the highest hole concentration in the p-EBL among the investigated devices. Consequently, the effective valence band barrier height (Φ_H) in Device B is decreased to 445.9 meV, leading to a high hole concentration in the active region.

As the Al composition in the insertion layer further increases in Device C, the barrier height (ΔE_{1b}) at interface (I_4) is reduced from 170.3 meV in Device B to 58.4 meV at the EBL/$Al_{0.55}Ga_{0.45}N$ interface (I_6) of Device C, as shown in Table 1. However, due to the large Al composition discontinuity between the $Al_{0.55}Ga_{0.45}N$ insertion layer and the p-$Al_{0.4}Ga_{0.6}N$ hole supplier, the barrier height at the $Al_{0.55}Ga_{0.45}N$/p-AlGaN interface (I_6) is obviously enhanced in Device C, making it difficult for holes to climb over this potential barrier (ΔE_{1a}) at I_5. As depicted in the inset of Fig. 3(d), the holes are confined at the $Al_{0.55}Ga_{0.45}N$/p-AlGaN interface (I_5), before crossing the stepped barrier (ΔE_{1a} and ΔE_{1b}) into the p-EBL. Under this circumstance,

Optical Materials EXPRESS

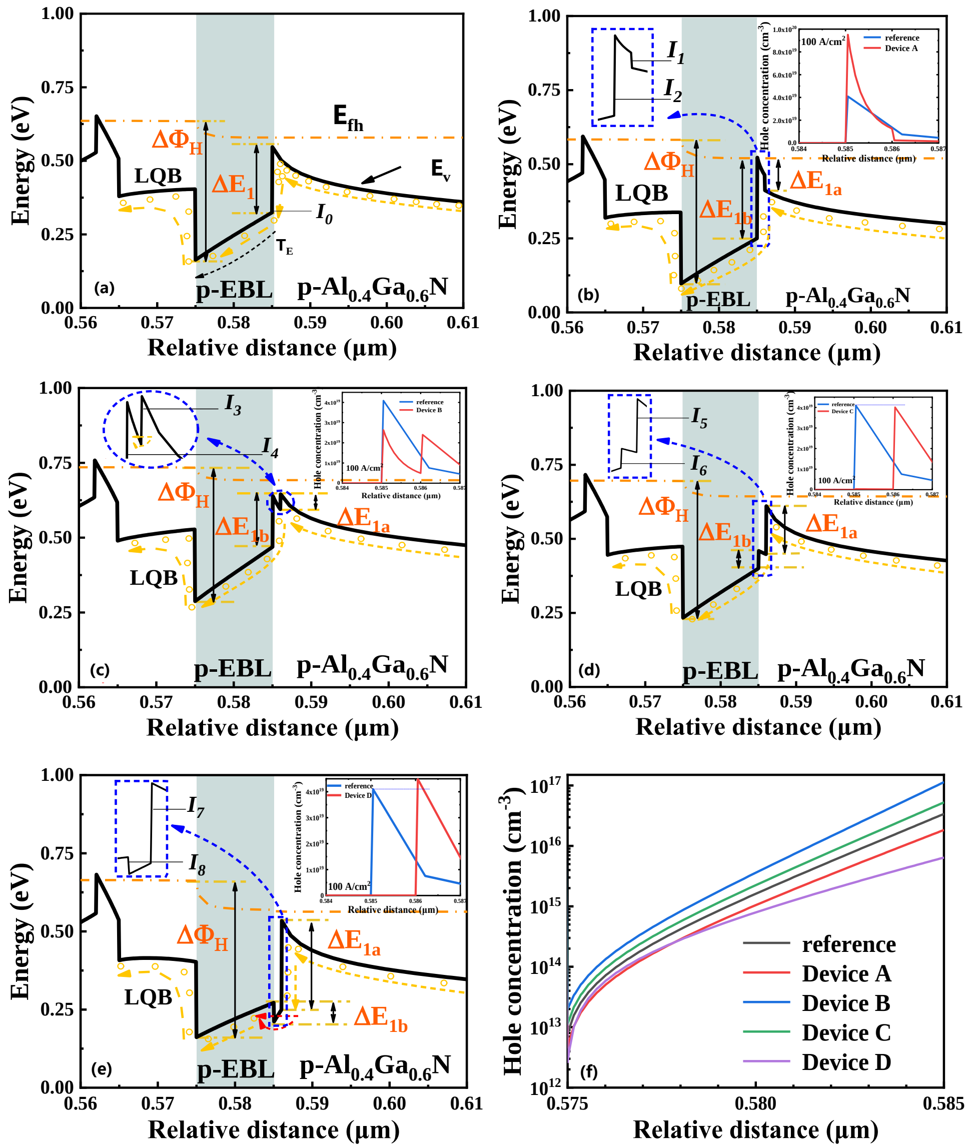

Fig. 3. The diagrams of valence band for (a) reference structure, Device (b) A, (c) B, (d) C, and (e) D in the area of LQB, EBL, and p-AlGaN layer at 100 A/cm^2. The inset figures depict the hole concentration in the thin insertion layer of the proposed device and reference structure. T_E is the thermionic emission process of holes. ΔE_1 denotes the barrier height at p-EBL/p-AlGaN interface in the reference structure. ΔE_{1a} and ΔE_{1b} represent the barrier height at $Al_xGa_{1-x}N$/p-AlGaN and p-EBL/$Al_xGa_{1-x}N$ interface in the proposed structure, respectively. Φ_H is the effective valence band barrier of the EBL. E_{fh} means the quasi-Fermi level for holes. I_0 is the p-EBL/p-AlGaN interface in reference structure. I_n and I_{n+1} are the $Al_xGa_{1-x}N$/p-AlGaN and p-EBL/$Al_xGa_{1-x}N$ interface, respectively. In detail, n is equal to 1, 3, 5, 7 in the Device A, B, C, and D, respectively. (f) The hole concentration in the EBL for all devices at the current density of 100 A/cm^2.

ΔE_{1i} in Eq. (2) for Device C ought to be redefined as the sum of ΔE_{1a} and ΔE_{1b}, which is smaller than ΔE_1 of the reference structure but larger than ΔE_{1i} of Device B (the max $\{\Delta E_{1a}, \Delta E_{1b}\}$). Consequently, the performance of Device C is improved in contrast to the reference structure, but it exhibits inferior EQE and optical power than Device B.

In Device D with an $Al_{0.65}Ga_{0.35}N$ insertion layer, the barrier height (ΔE_{1a}) of 314.7 meV at the $Al_{0.65}Ga_{0.35}N$/p-AlGaN interface (I_7) becomes the dominant reason that limits hole injection into the p-EBL, due to the larger valence band offset between $Al_{0.65}Ga_{0.35}N$ insertion layer and p-$Al_{0.4}Ga_{0.6}N$ hole supplier than that between p-EBL and the $Al_{0.65}Ga_{0.35}N$ insertion layer. As depicted in the inset of Fig. 3(e), a large density of holes is restricted at the $Al_{0.65}Ga_{0.35}N$/p-AlGaN interface (I_7), leading to the lowest hole concentration and largest barrier height of 499.4 meV at the p-EBL as well as minimized hole injection into the active layer at a forward current density of 100 A/cm^2. Therefore, Device D features the worst optical power and external quantum efficiency.

On the other hand, it has been reported that the origin of efficiency droop effect is also related to the electron leakage [33,34]. To explore the electron blocking capability of the proposed structures, we plot the conduction band diagrams of the p-EBL for the investigated devices, as displayed in Fig. 4(a). The energy level difference between the highest point for the conduction band and the quasi-Fermi level for the electrons is defined as the effective conduction band height (Φ_C) of p-EBL, of which the values were marked in the Table 1. Besides, the normalized electron current density for the investigated devices at the current density of 100 A/cm^2 is also depicted in Fig. 4(b). In the reference structure, the energy band discontinuity between p-EBL and p-AlGaN hole supplier tends to bend the conduction band of p-EBL downwards. Yet the polarization-related negative charges at p-EBL/p-AlGaN interface can deplete the electrons in the vicinity of the p-EBL, causing an upward bending of conduction band. The polarization-induced charge density at the p-EBL(top)/$Al_xGa_{1-x}N$(bottom) heterointerface is calculated by the equation:

$$\sigma = \frac{\{P_{sp}(top) + P_{pz}(top)\} - \{P_{sp}(bottom) + P_{pz}(bottom)\}}{q} * \alpha, \quad (5)$$

in which q is elementary charge, α is the polarization level of AlGaN ternary alloy. The spontaneous polarization (P_{sp}) in the AlGaN alloy and piezoelectric polarization (P_{pz}) between the p-EBL and $Al_xGa_{1-x}N$ insertion layer can be calculated according to Ref. [35,36]. The values of polarization-induced sheet charge density of the investigated devices at the p-EBL/$Al_xGa_{1-x}N$ interface are marked in Table 1. The combined effect of these two factors determines the effective conduction band barrier height (Φ_C) of p-EBL.

As for Device A shown in Fig. 4(a), since the influence of the energy band discontinuity between p-EBL and $Al_{0.35}Ga_{0.65}N$ insertion layer outweighs that of the negative sheet charges of $-6.4 \times 10^{16}\,m^{-2}$ at the p-EBL/$Al_{0.35}Ga_{0.65}N$ interface, it can be observed that Φ_C in Device A is decreased to 363.61 meV, thus leading to an increased electron leakage current compared with reference sample. In contrast, the effective conduction band barrier height of p-EBL for Device B is increased to 408.1 meV. It is not only due to the smaller energy band nonalignment between p-EBL and $Al_{0.45}Ga_{0.55}N$ insertion layer compared with reference sample, but also because the polarization-related negative sheet charges at p-EBL/$Al_{0.45}Ga_{0.55}N$ interface elevate the Φ_C of p-EBL. It is indicated that the polarization-related charges at the p-EBL/$Al_{0.45}Ga_{0.55}N$ interface start playing a major part in the Φ_C of p-EBL, as the Al composition in the insertion layer increases. Accordingly, although the energy band discontinuity between p-EBL and $Al_{0.55}Ga_{0.45}N$ insertion layer in Device C is further reduced, the Φ_C of Device C (383.9 meV) is smaller than that of Device B (408.1 meV) due to the lower negative sheet charge density at the p-EBL/$Al_{0.55}Ga_{0.45}N$ interface of Device C than Device B (the charge density at p-EBL/$Al_xGa_{1-x}N$ interface of Device B and Device C is $-4 \times 10^{16}\,m^{-2}$ and $-1.4 \times 10^{16}\,m^{-2}$, respectively) [37,38]. Thus, Device B exhibited an enhanced electron confinement capability and a suppressed electron leakage than Device C.

Optical Materials EXPRESS

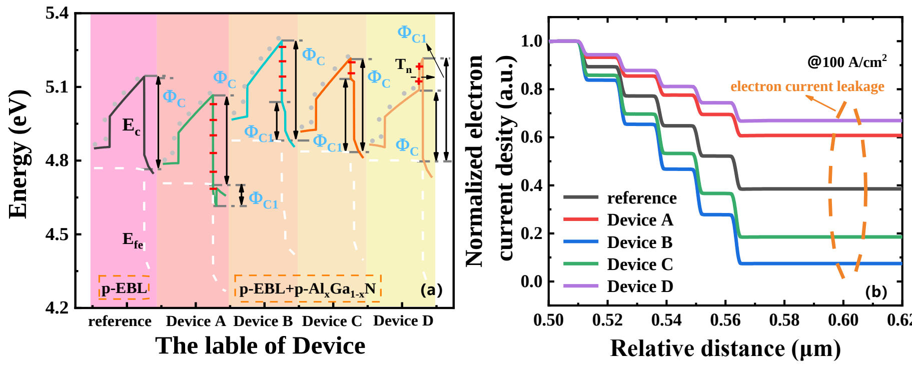

Fig. 4. (a) Conduction band diagram for reference structure, Device A, B, C, and D between LQB and p-$Al_{0.4}Ga_{0.6}N$ hole supplier at 100 A/cm^2. E_c and E_{fe} mean the conduction band and the quasi-Fermi level for electrons, respectively. Φ_{c1} is the effective barrier height for electrons in the insertion layer. (b) Normalized electron density for the investigated devices at the current density of 100 A/cm^2.

With further increased Al composition in the insertion layer, we can find that the Φ_C of p-EBL in Device D is remarkably decreased to 287.3 meV, which is driven by the polarization-related positive charges of $1.5 \times 10^{16}\,m^{-2}$ at the p-EBL/$Al_{0.65}Ga_{0.35}N$ interface. Please note that the Φ_{C1} (421.9 meV) of the $Al_{0.65}Ga_{0.35}N$ insertion layer is larger than Φ_C (287.3 meV) of the p-EBL, which can play a key role in preventing the electrons from transporting into the p-type region. However, the thickness of the $Al_{0.65}Ga_{0.35}N$ insertion layer is extremely thin, which results in numerous electron leakage into the p-type hole supplier through tunneling process (T_n). Therefore, Device D is characterized by the largest electron leakage and the most serious efficiency droop among the investigated devices. To sum up, it is of utmost significance to properly design the thickness and Al composition of the insertion layer for the purpose of reducing the electron leakage current and alleviating the efficiency droop of AlGaN-based DUV LEDs.

To further verify the effect of the thin insertion layer on the device performance, we extract the wavefunction overlap of the electrons and holes in the 3rd well, the integration of the carrier concentration in the active region, the horizontal carrier concentration in the last quantum well (LQW) at 100 A/cm^2 and radiative recombination rates in the MQW for the investigated devices, as shown in Fig. 5(a)–5(d), respectively. The position of the radiative recombination rate profile for the proposed structures is shifted rightwards by 3 nm in comparison with the reference structure. As shown in Fig. 5(a), there is no significant difference between the proposed devices (Device A, B, C, and D) and the reference structure in the value of electron and hole wavefunction overlap, indicating that the effect of the wavefunction overlap on the radiative recombination rates can be neglected among the investigated devices in this work. The carrier concentration in the active region is another essential factor that influences the radiative recombination rates. It can be seen from Fig. 5(b) that the electron concentration in the LQW is higher than that in other quantum wells. The asymmetry of electron distribution among the quantum wells is mainly attributed to the fact that electrons feature higher mobility and smaller effective mass than holes, which results in non-synchronized electron and hole transport behavior. Moreover, the tilted energy band of the quantum barriers induced by the polarization field further weakens the quantum confinement of the quantum barriers. Therefore, the electrons tend to accumulate in the last quantum well adjacent to the p-type electron blocking layer with higher effective barrier for electrons, which reflects electrons back to the active region. Furthermore, Device A possesses lower carrier concentration than the reference structure, resulting in an inferior

Optical Materials EXPRESS

radiative recombination rate to that of the reference structure. The reduced carrier concentration is attributed to the smaller Φ_C and ΔE_{1b} in Device A. On the contrary, the carrier concentration of Device B and C is higher than that of reference structure, thanks to the reduced barrier height (ΔE_{1b}) and enhanced Φ_C of p-EBL with high-Al-composition insertion layers. Specifically, Device B exhibits a higher hole concentration in the active region and a higher horizontal hole concentration in the LQW compared with Device C, since ΔE_{1b} of Device B is lower than that of Device C. The electron confinement capability is also boosted for Device B due to the larger Φ_C of Device B than Device C (see Table 1), raising the electron concentration in the MQW. As for Device D, although the lateral electron distribution in the LQW is slightly homogenized by the high barrier ($\Phi_{C1} = 421.9$ meV) for electron between p-EBL and p-AlGaN hole supplier [39], as shown in Fig. 4(a) and Fig. 5(c), the rate of radiative recombination in the active region is minimized due to the severe electron leakage and low hole injection, leading to degraded optical power and efficiency droop.

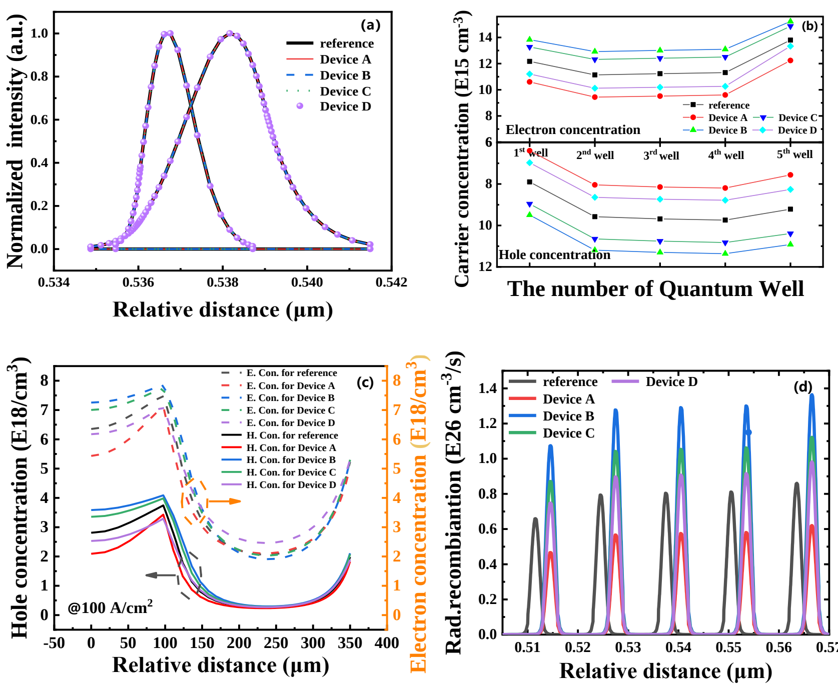

Fig. 5. (a) The wavefunction overlap of the electrons and holes in the 3rd quantum well for the investigated devices at the current density of 100 A/cm^2. (b) The integration of hole concentration of each well in the active region. (c) The hole and electron concentration (H. Con. and E. Con. are their shortened form) in the LQW for all devices at the current density of 100 A/cm^2. (d) Recombination rate profile in the active region.

4. Conclusion

To summarize, we investigate the hole transport behavior across the p-EBL/p-AlGaN interface and propose a thin $Al_xGa_{1-x}N$ insertion layer between p-EBL and p-type hole supplier to improve hole injection efficiency. By adjusting the Al composition in the insertion layer, we systematically investigated the influence of the $Al_xGa_{1-x}N$ insertion layer ($x = 0.35$, 0.45, 0.55, and 0.65) on the barrier height at p-EBL/$Al_xGa_{1-x}N$ interface. The insertion layer with appropriate Al composition can reduce the barrier height at p-EBL/$Al_xGa_{1-x}N$ interface, which contributes to enhancing the hole current density from hole supplier into the active region. On the other hand, the negative sheet charges introduced by the $Al_xGa_{1-x}N$ insertion layer can give rise to the enhanced barrier height for electrons, and thus improving the electron confinement of p-EBL. With the combined effect from the enhanced Φ_C and the reduced barrier height at the p-EBL/p-AlGaN interface, the device with $Al_{0.45}Ga_{0.55}N$ insertion layer exhibits a significant improvement in the optical power by 40.5%. Therefore, we believe that the p-EBL/$Al_xGa_{1-x}N$/p-AlGaN structure provides a potential approach to achieve DUV LEDs with satisfactory luminous efficiency.

Funding. Shenzhen Science and Technology Program (GJHZ20210705142537002, JCYJ20210324141212030); Basic and Applied Basic Research Foundation of Guangdong Province (2020A1515111018, 2023A1515011142); Natural Science Foundation of Shandong Province (ZR2020QF079); Qilu Young Scholar program (11500089963075).

Acknowledgments. The authors thank staff from Simucal Inc. and Changsheng Xia form Sinopeda Technology Co. Ltd. for their technical and fruitful discussion.

Disclosures. The authors declare no conflicts of interest.

Data availability. Data underlying the results presented in this paper are not publicly available at this time but may be obtained from the authors upon reasonable request.

References

1. N. Alfaraj, J. Min, C. H. Kang, A. A. Alatawi, D. Priante, R. C. Subedi, M. Tangi, T. K. Ng, and B. S. Ooi, "Deep-ultraviolet integrated photonic and optoelectronic devices: A prospect of the hybridization of group III-nitrides, III-oxides, and two-dimensional materials," J. Semicond. **40**(12), 121801 (2019).
2. H. Hirayama, N. Maeda, S. Fujikawa, S. Toyoda, and N. Kamata, "Recent progress and future prospects of AlGaN-based high-efficiency deep-ultraviolet light-emitting diodes," Jpn. J. Appl. Phys. **53**(10), 100209 (2014).
3. M. S. Shur and R. Gaska, "Deep-Ultraviolet light-emitting diodes," IEEE Trans. Electron Devices **57**(1), 12–25 (2010).
4. Z. Ren, H. Yu, Z. Liu, D. Wang, C. Xing, H. Zhang, C. Huang, S. Long, and H. Sun, "Band engineering of III-nitride-based deep-ultraviolet light-emitting diodes: a review," J. Phys. D: Appl. Phys. **53**(7), 073002 (2020).
5. Y. Peng, R. Liang, Y. Mou, J. Dai, M. Chen, and X. Luo, "Progress and perspective of near-ultraviolet and deep-ultraviolet light-emitting diode packaging technologies," J. Electron. Packag. **141**(4), 040804 (2019).
6. Y. Chen, J. Ben, F. Xu, J. Li, Y. Chen, X. Sun, and D. Li, "Review on the Progress of AlGaN-based Ultraviolet Light-Emitting Diodes," Fundamental Research **1**(6), 717–734 (2021).
7. M. Shatalov, R. Jain, T. Saxena, A. Dobrinsky, and M. Shur, "Development of Deep UV LEDs and Current Problems in Material and Device Technology," Semicond. Semimet. **96**, 45–83 (2017).
8. T. F. K. Weatherley, W. Liu, V. Osokin, D. T. L. Alexander, R. A. Taylor, J. Carlin, R. Butté, and N. Grandjean, "Imaging Nonradiative Point Defects Buried in Quantum Wells Using Cathodoluminescence," Nano Lett. **21**(12), 5217–5224 (2021).
9. L. Li, Y. Zhang, S. Xu, W. Bi, Z. Zhang, and H. Kuo, "On the Hole Injection for III-Nitride Based Deep Ultraviolet Light-Emitting Diodes," Materials **10**(10), 1221 (2017).
10. H. Hirayama, Y. Tsukada, T. Maeda, and N. Kamata, "Marked Enhancement in the Efficiency of Deep-Ultraviolet AlGaN Light-Emitting Diodes by Using a Multiquantum-Barrier Electron Blocking Layer," Appl. Phys. Express **3**(3), 031002 (2010).
11. J. Hu, J. Zhang, Y. Zhang, H. Zhang, H. Long, Q. Chen, M. Shan, S. Du, J. Dai, and C. Chen, "Enhanced Performance of AlGaN-Based Deep Ultraviolet Light-Emitting Diodes with Chirped Superlattice Electron Deceleration Layer," Nanoscale Res. Lett. **14**(1), 347 (2019).
12. M. Liu, Y. Ji, H. Zhou, C. Xia, Z. Zhang, and C. Liu, "Sheet Charge Engineering Towards an Efficient Hole Injection in 290 nm Deep Ultraviolet Light-Emitting Diodes," IEEE Photonics J. **13**(4), 1–8 (2021).
13. J. Piprek and S. Li, "Electron leakage effects on GaN-based light-emitting diodes," Opt. Quantum Electron. **42**(2), 89–95 (2010).
14. K. B. Lee, P. J. Parbrook, T. Wang, J. Bai, F. Ranalli, R. J. Airey, and G. Hill, "Effect of the AlGaN electron blocking layer thickness on the performance of AlGaN-based ultraviolet light-emitting diodes," J. Cryst. Growth **311**(10), 2857–2859 (2009).
15. T. Jamil, M. Usman, and H. Jamal, "Sandwiching electron blocking layer with p-AlInN layer to enhance hole injection in AlGaN-based deep ultraviolet light-emitting diodes," Mater. Res. Bull. **142**, 111389 (2021).
16. Z. Liu, Y. Lu, Y. Wang, R. Lin, C. Xiong, and X. Li, "Polarization Modulation at Last Quantum Barrier for High Efficiency AlGaN-Based UV LED," IEEE Photonics J. **14**(1), 1–8 (2022).
17. J. Piprek and Z. M. Simon Li, "Sensitivity analysis of electron leakage in III-nitride light-emitting diodes," Appl. Phys. Lett. **102**(13), 131103 (2013).

Optical Materials EXPRESS

18. L. Wang, W. He, T. Zheng, Z. Chen, and S. Zheng, “Enhanced optical performance of AlGaN-based deep-ultraviolet light-emitting diode with m-shaped hole blocking layer and w-shaped electron blocking layer,” Superlattices Microstruct. **133**, 106188 (2019).
19. Z. Zhang, S. Huang Chen, Y. Zhang, L. Li, S. Wang, K. Tian, C. Chu, M. Fang, H. Kuo, and W. Bi, “Hole Transport Manipulation To Improve the Hole Injection for Deep Ultraviolet Light-Emitting Diodes,” ACS Photonics **4**(7), 1846–1850 (2017).
20. M. Usman, T. Jamil, S. Malik, and H. Jamal, “Designing anti-trapezoidal electron blocking layer for the amelioration of AlGaN-based deep ultraviolet light-emitting diodes internal quantum efficiency,” Optik **232**, 166528 (2021).
21. C. Chu, K. Tian, M. Fang, Y. Zhang, L. Li, W. Bi, and Z. Zhang, “On the $Al_xGa_{1-x}N/Al_yGa_{1-y}N/Al_xGa_{1-x}N$ (x > y) p-electron blocking layer to improve the hole injection for AlGaN based deep ultraviolet light-emitting diodes,” Superlattices Microstruct. **113**, 472–477 (2018).
22. P. Sun, X. Bao, S. Liu, C. Ye, Z. Yuan, Y. Wu, S. Li, and J. Kang, “Advantages of AlGaN-based deep ultraviolet light-emitting diodes with a superlattice electron blocking layer,” Superlattices Microstruct. **85**, 59–66 (2015).
23. Q. Cai, H. You, H. Guo, J. Wang, B. Liu, Z. Xie, D. Chen, H. Lu, Y. Zheng, and R. Zhang, “Progress on AlGaN-based solar-blind ultraviolet photodetectors and focal plane arrays,” Light: Sci. Appl. **10**(1), 94 (2021).
24. Y. Li, S. Chen, W. Tian, Z. Wu, Y. Fang, J. Dai, and C. Chen, “Advantages of AlGaN-Based 310-nm UV Light-Emitting Diodes With Al Content Graded AlGaN Electron Blocking Layers,” IEEE Photonics J. **5**(4), 8200309 (2013).
25. N. U. Islam, M. Usman, S. Khan, T. Jamil, S. Rasheed, S. Ali, and S. Saeed, “Remarkable efficiency improvement in AlGaN-based ultraviolet light-emitting diodes using graded last quantum barrier,” Optik **248**, 168212 (2021).
26. M. Liu and C. Liu, “Enhanced Carrier Injection in AlGaN-Based Deep Ultraviolet Light-Emitting Diodes by Polarization Engineering at the LQB/p-EBL Interface,” IEEE Photonics J. **14**(3), 1–5 (2022).
27. Z. Zhang, W. Liu, S. T. Tan, Y. Ji, L. Wang, B. Zhu, Y. Zhang, S. Lu, X. Zhang, N. Hasanov, X. W. Sun, and H. V. Demir, “A hole accelerator for InGaN/GaN light-emitting diodes,” Appl. Phys. Lett. **105**(15), 153503 (2014).
28. Z. Liu, H. Yu, Z. Ren, J. Dai, C. Chen, and H. Sun, “Polarization-engineered AlGaN last quantum barrier for efficient deep-ultraviolet light-emitting diodes,” Semicond. Sci. Technol. **35**(7), 075021 (2020).
29. I. Vurgaftman, J. R. Meyer, and L. R. Ram-Mohan, “Band parameters for III–V compound semiconductors and their alloys,” J. Appl. Phys. **89**(11), 5815–5875 (2001).
30. C. S. Xia, Z. M. Simon Li, Y. Sheng, L. W. Cheng, W. D. Hu, and W. Lu, “Simulation of InGaN/GaN light-emitting diodes with a non-local quantum well transport model,” Opt. Quantum Electron. **45**(7), 597–604 (2013).
31. Z. Zhang, Y. Zhang, W. Bi, C. Geng, S. Xu, H. V. Demir, and X. W. Sun, “A charge inverter for III-nitride light-emitting diodes,” Appl. Phys. Lett. **108**(13), 133502 (2016).
32. D. Zhang, C. Chu, K. Tian, J. Kou, W. Bi, Y. Zhang, and Z. Zhang, “Improving hole injection from p-EBL down to the end of active region by simply playing with polarization effect for AlGaN based DUV light-emitting diodes,” AIP Adv. **10**(6), 065032 (2020).
33. D. S. Meyaard, G. Lin, J. Cho, E. Fred Schubert, H. Shim, S. Han, M. Kim, C. Sone, and Y. Sun Kim, “Identifying the cause of the efficiency droop in GaInN light-emitting diodes by correlating the onset of high injection with the onset of the efficiency droop,” Appl. Phys. Lett. **102**(25), 251114 (2013).
34. J. Piprek, “Efficiency droop in nitride-based light-emitting diodes,” Phys. Status Solidi A **207**(10), 2217–2225 (2010).
35. V. Fiorentini, F. Bernardini, and O. Ambacher, “Evidence for nonlinear macroscopic polarization in III–V nitride alloy heterostructures,” Appl. Phys. Lett. **80**(7), 1204–1206 (2002).
36. F. Bernardini, V. Fiorentini, and D. Vanderbilt, “Spontaneous polarization and piezoelectric constants of III-V nitrides,” Phys. Rev. B **56**(16), R10024 (1997).
37. T. Yu and K. F. Brennan, “Theoretical study of the two-dimensional electron mobility in strained III-nitride heterostructures,” J. Appl. Phys. **89**(7), 3827–3834 (2001).
38. S. Heikman, S. Keller, Y. Wu, JS. Speck, SP. DenBaars, and UK. Mishra, “Polarization effects in AlGaN/GaN and GaN/AlGaN/GaN heterostructures,” J. Appl. Phys. **93**(12), 10114–10118 (2003).
39. J. Che, H. Shao, L. Chang, J. Kou, K. Tian, C. Chu, Y. Zhang, W. Bi, and Z. Zhang, “Doping-induced energy barriers to improve the current spreading effect for AlGaN-based ultraviolet-B light-emitting diodes,” IEEE Electron Device Lett. **41**(7), 1 (2020).